Received: November 24, 2020. Revised: May 19, 2021. Accepted: June 7, 2021. Published: June 19, 2021.

Characterization Of ZnS/GaAs Nanostructures Grown By RF Magnetron Sputtering

J. Diaz-Reyes[1], O. Zaca-Moran[1], J. Martinez-Juárez[2], R. Castillo-Ojeda[3], M. Galvan-Arellano[4], E. Lopez-Cruz[5] and E. Flores-Mena[6]

[1] Centro de Investigación en Biotecnología Aplicada, Instituto Politécnico Nacional. Tepetitla, México

[2] Centro de Investigación en Dispositivos Semiconductores, ICUAP, Benemérita Universidad Autónoma de Puebla. Puebla. México

[3] Universidad Politécnica de Pachuca. Municipio de Zempoala, Hidalgo. México

[4] Depto. de Ingeniería Eléctrica, SEES. CINVESTAV-IPN, México, D.F. México

[5] Instituto de Física "Luis Rivera Terrazas". Benemérita Universidad Autónoma de Puebla. Puebla, México

[6] Facultad de Ciencias de la Electrónica, Benemérita Universidad Autónoma de Puebla, Puebla, México

***Abstract*—Zinc sulfide (ZnS) is one of the most important II-VI group semiconductors, with a wide direct band gap of 3.8 eV has been extensively investigated and used in electroluminescent devices, flat panel displays, infrared windows, sensors, and lasers. To explore the possibility of using it in electroluminescent devices, a study of the structural and optical properties of the host material is an important step. Based on the above criterion, the structural and optical properties of ZnS films have been studied in the present work. ZnS thin films were grown on (001) GaAs substrates at different temperatures by RF magnetron sputtering. The stoichiometry chemical was determined by Energy-dispersive X-ray spectroscopy (EDS). The XRD analysis and Raman scattering reveals that deposited films showed wurzite crystalline phase. The average crystallite size range of the film was from 11.15 to 34.95 nm, which was determined using the Scherrer formula. Besides it made an experimental study on first- and second-order Raman scattering of wurtzite. The 300 K photoluminescence presents a visible radiative band associates to vacancies of zinc and sulphur.**

Keywords—II-VII semiconductor compounds, X-ray, SEM-EDS, photoluminescence, Raman Sputtering,

I. Introduction

Wide band gap semiconductors containing a great number of defects, surface states or doped with optically active luminescence centres, have created new opportunities for optical studies and development of applications [1,2]. Deep-level energy bands allow semiconductor materials to emit at longer wavelengths. Then it is possible to fabricate LEDs from these materials [3]. Nevertheless for some uses, it has been shown that such materials must be grown with a monocrystalline structure and a smooth surface [4]. Zinc sulfide (ZnS), an important semiconductor compound of the IIB-VI groups, is mostly found in one of two structural forms cubic sphalerite or hexagonal wurtzite, which have wide band gaps of 3.54 eV and 3.80 eV, respectively at 300 K [5]. It is a well-known luminescence material having prominent and promising applications in displays, sensors and blue-light emission device application [6]. The II-VI semiconductor ZnS is used in many applications primarily for its luminescent properties. It has a direct band gap of 3.8eV and a small exciton Bohr radius of 2.5 nm. Owing to its wide band gap, it is used in violet and blue regions.

ZnS has been grown on Si and GaAs substrates [6,7]. It is closely lattice matched with Si (0.2%), which makes it a promising material for the integration in optoelectronic devices on Si substrates. However, ZnS and Si exhibit a large thermal expansion coefficient mismatch (13.6%) while the thermal expansion coefficients of ZnS and GaAs are better matched (10.5%). Furthermore, ZnS and GaAs exhibit a large lattice constant mismatch (4.5%). Growth of ZnS thin films has been conventionally done using several methods, such as chemical vapour deposition (CVD) [8], molecular beam epitaxy (MBE) [9], atomic layer epitaxy (ALE) [10], metallorganic chemical vapour deposition (MOCVD) [11], successive ionic layer adsorption and reaction methods (SILAR) [10], metallorganic vapour phase epitaxy (MOVPE) [12], pulsed laser deposition (PLD) [13] and electron induced epitaxy (EIE) [7].

The main advantage of the nanostructures is their size dependent property. As the size approaches that of the Bohr radius, quantum confinement effects result in the blue shifting of the band gap [3]. The Bohr radius of ZnS is 2.5 nm [14]. In this paper, the diameter of ZnS nanostructures is 11.15–45.83 nm, which is much larger than the Bohr radius as well as the excitonic diameter. Therefore, the quantum confinement effect may not be significant in these nanostructures. The recombination properties of the ZnS nanostructures differ from those of bulk ZnS due to the larger surface to volume ratio. With reduction in size, the surface area plays a dominant role in the material properties, and the presence of many surface defects may also affect the emission properties of ZnS nanostructures.

Recently, it has used rf magnetron sputtering to grow a variety of materials including GaAs, Ge, Si and some other combinations of them [15]. This technique can deposit large area films of well-controlled compositions economically and the growth rate is high enough for thick films and low enough for ultrathin films by changing the sputtering time [16]. In the present work, we report the growth and characterization studies of ZnS thin films on GaAs (001) deposited at various temperatures (180–630°C) using a rf planar magnetron

sputtering system. Effects of temperature during the sputtering with Ar plasma on crystalline quality, particle size and morphology of the thin films were studied by SEM-EDS, X-ray diffraction, Raman spectroscopy and room temperature photoluminescence. Raman and photoluminescence spectroscopy are powerful and non-destructive optical tools to study vibrational and optical properties of ZnS nanostructures. ZnO is a Raman active material with a hexagonal wurtzite structure that belongs to the space group C_{6v} (6 mm).

II. EXPERIMENTAL DETAILS

The used substrates were (100) GaAs semi-insulating doped with chromium of 10x10 mm^2 of area, with 50 mm separation between the target and substrate. The direct growth of ZnS on GaAs substrates is advantageous because of not only it reduces the polar–nonpolar interface problems but also the thermal expansion coefficients are matched. The base pressure inside the chamber was better than $7.5x10^{-7}$ mbar. Plasma of Ar (99.999%) was created to sputter a 100 mm diameter, water-cooled, ZnS (99.99%) target mounted under a planar magnetron. The RF power was 50W. The sputtering time was about 2.0 h for all deposited samples. During sputtering process the Ar-pressure was maintained at $15x10^{-3}$ mbar. A partial pressure of hydrogen gas was introduced to the growth chamber during 30 min at room temperature before thin film deposition on the substrate. This gas partial pressure condition was maintained during the temperature ramp from room temperature to growth temperature. Grown samples are presented in Table I. The crystalline phase and structure of the films was determined with a Bruker D8 Discover diffractometer using the copper Kα radiation (λ=1.5406 Å) at 40 kV and 40 mA with parallel beam geometry. Raman scattering experiments were performed at room temperature using the 6328 Å line of a He-Ne laser at normal incidence for excitation. The laser light was focused to a diameter of 6.0 µm at the sample using a 50x (numerical aperture 0.9) microscope objective. The nominal laser power used in these measurements was 20 mW. Scattered light was analyzed using a micro-Raman system (Lambram model of Dilor), a holographic notch filter made by Kaiser Optical System, Inc. (model superNotch-Plus), a 256x1024-pixel CCD used as detector cooled to 140 K using liquid nitrogen, and two interchangeable gratings (600 and 1800 g/mm). Typical spectrum acquisition time was limited to 60 s to minimize the sample heating effects. Absolute spectral feature position calibration to better than 0.5 cm^{-1} was performed using the observed position of Si which is shifted by 521.2 cm^{-1} from the excitation line. Room-temperature photoluminescence was taken with a solid state laser 325 nm with 60 mW as excitation source and a SCIENCETECH 9040 monochromator was used to perform the sweep of wavelength at room and low temperature in a cryostat CRYOGENICS.

III. EXPERIMENTAL DETAILS AND DISCUSSION

Figure 1 shows XRD diffractograms from some the polycrystalline ZnS nanostructures grown on GaAs (001). It is observed from XRD patterns that ZnS films deposited even at low temperature are in crystalline nature, which present two

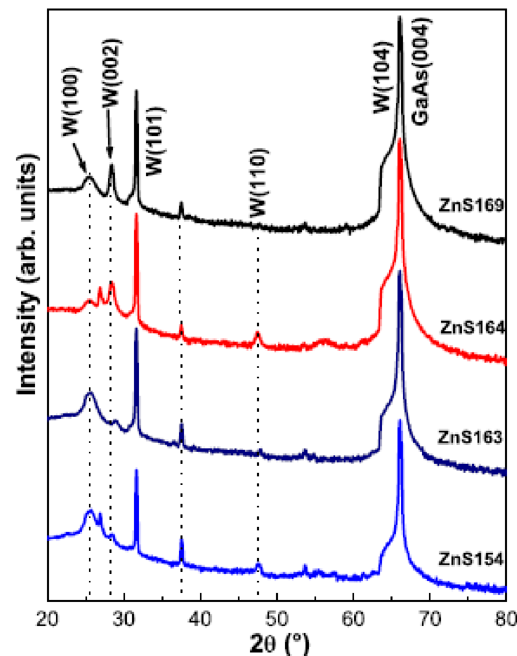

Fig. 1. X-ray patterns of the ZnS films synthesized by sputtering.

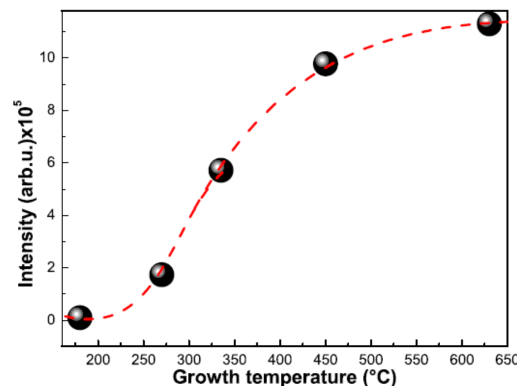

Fig. 2. (004) GaAs peak intensity versus growth temperature.

peaks dominant at 31.59 and 65.94°. This may be attributed to the fact that the crystalline GaAs substrate facilitates the growth of crystalline ZnS thin films and their crystal lattice orientation is initiated on the GaAs substrates at room temperature. It can be seen that each peak corresponds fairly will with data of ZnS marked in the software DICVOL04 data. The obtained structural parameters with the software DICVOL04 data are in good agreement with the published. From this close agreement, it is confirmed that as-deposited ZnS films for all the grown temperatures belong to the wurtzite crystal system. The X-ray pattern of as-deposited ZnS film is described in the C_{6v} *(6mm)* and whose lattice parameters were calculated using the software DICVOL04, obtaining the following lattice parameters values: a = 3.81 Å and c/a = 1.62 Å, which are in agreement with the reported values [9]. In all cases the samples present the same reflections and some of them can be assigned. There is a peak dominant highly intense from the ZnS/GaAs nanostructures at 65.94°, which is formed by two peaks which correspond to the wurtzite hexagonal (104) reflection of ZnS and zinc blende (004) GaAs reflection has

come from the substrate material, as will be discussed below. As is observed from the X-ray diffractograms the intensity of the peaks clearly increases as the grown temperature is increased, in particular for the peak at 65.94° of sample ZnS169 that is seven order of magnitude higher compared with ZnS154, see Fig. 1, which is shown in Fig. 2. It suggests that the films ZnS154 and ZnS163 are lightly less preferentially oriented than the samples that the ZnS164 and ZnS169. Other peaks are observed on the diffractograms of the samples. The hexagonal (101) reflection is identified at 31.74°, hexagonal (002) reflection is observed at 28.45° and hexagonal (100) at 25.3°. It is clear that increasing the temperature improves the crystalline structure in thin films [17], since main peak increase as the grown temperature is increased, which implies that the crystallinity is better as previously mentioned. Some authors have reported that low growth temperature (<335 ºC) the ZnS results in a cubic structure for the thin films [18], but in this case did not occur and all nanostructures were wurtzite type. In order to obtain more structural information, the mean grain size (D) of the deposited nanofilms was evaluated using the Scherrer equation [19]. The mean grain size was calculated from hexagonal (101) reflection of ZnS for the all samples. The mean grain sizes of the nanostructures are presented in Table 1. These results show that the grain size remained almost constant (~33 nm) for the temperature range from 180 to 450ºC, to higher temperatures the grain size diminishes as can be observed in Table 1. The grain size as determined by XRD for each sample is summarized in Table 1. Besides, in Table 1 present the film thicknesses grown by rf-sputtering.

TABLE I. RESULTS OF THE ANALYSIS BY EDS OF THE SAMPLES. THICKNESS OF THE FILMS AND GRAIN SIZE OF NANOPARTICLES OF ZNS STUDIED IN THIS WORK.

Sample	T_G (°)	S atomic percent (%)	Zn atomic percent (%)	Films thickness by SEM (nm)	Size grain by XRD (nm)
ZnS140	180	50.21	49.79	865.3	31.18
ZnS154	270	49.01	50.99	845.8	34.95
ZnS163	335	47.07	52.93	887.1	31.31
ZnS164	450	38.89	61.11	828.3	33.30
ZnS169	630	32.18	67.18	801.2	11.15

The composition of the samples is analysed by EDS to check the presence of any unintentional impurities. The EDS spectra (Fig. 3) indicate the presence of oxygen in the samples along with zinc and sulphur. By XPS analysis has showed that oxygen ions are present in the sample in the form of O^{2-} ions [20] that may produce ZnO. The chemical route for the oxidation reaction of ZnS to ZnO can be represented as $ZnS+3/2O_2 \rightarrow ZnO + SO_2$. Oxidation of ZnS to ZnO occurs at high temperatures such as 550°C and 600°C is already reported by many groups [21,22]. Since the temperature during synthesis and air drying in the present case is low, this conversion may have happened only at a very low percentage so that the presence of ZnO could not be detected in XRD. However, these oxygen ions can form trap levels in the band gap, resulting in several transitions contributing to luminescence. Thus it appears that oxygen has replaced sulphur at a few random points of the ZnS lattice. Figure 3a shows the bulk-EDS spectra of the ZnS nanostructure grown at 270°C. The EDS spectrum indicates that besides Zn and S, the samples contain a significant amount of potassium, gold and oxygen. Fig. 3b shows the typical bulk-EDS spectrum of the sample ZnS sample grown at 630ºC. This sample contains a large amount of arsenic and gallium, besides a significant amount of oxygen that allows forming the ZnO. The results of such measurements for the zinc and sulphur are shown in Table I. From these results is observed that the sample ZnS154 is the one that has a good stoichiometric compound and that starting from it a higher temperature gives a greater presence of zinc in the material and an absence of sulphur. Continuing with the consideration that each unit cell contains two zinc atoms and two sulphur atoms, then when a stoichiometric deviation of ideal unit cell occurs it could establish a correspondence between vacancies or interstices of some of the elements (V_S, V_{Zn}, Zn_i, S_i). From Table 1 observes that the sample ZnS169 contains a lower sulphur concentration, which indicates that it has a higher structural defects concentration.

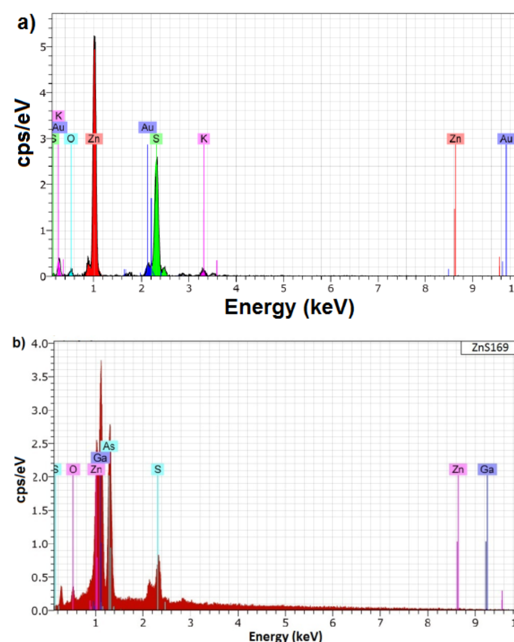

Fig. 3. Bulk EDS spectrum of ZnS samples: a) ZnS154 and b) ZnS169 samples.

The composition of the samples is analysed by EDS to check the presence of any unintentional impurities. The EDS spectra (Fig. 3) indicate the presence of oxygen in the samples along with zinc and sulphur. By XPS analysis has showed that oxygen ions are present in the sample in the form of O^{2-} ions [20] that may produce ZnO. The chemical route for the oxidation reaction of ZnS to ZnO can be represented as $ZnS+3/2O_2 \rightarrow ZnO + SO_2$. Oxidation of ZnS to ZnO occurs at high temperatures such as 550°C and 600°C is already reported by many groups [21,22]. Since the temperature during synthesis and air drying in the present case is low, this conversion may have happened only at a very low percentage so that the presence of ZnO could not be detected in XRD. However, these oxygen ions can form trap levels in the band gap, resulting in several transitions contributing to luminescence. Thus it appears that oxygen has replaced sulphur at a few random points of the ZnS lattice.

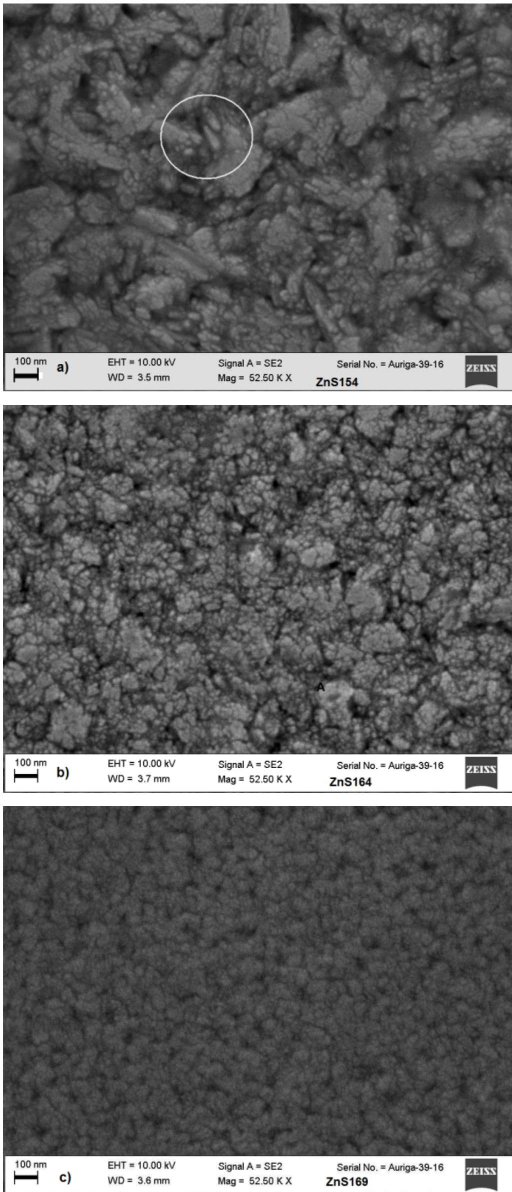

Fig. 4. SEM images of ZnS nanostructures samples with growth temperature: (a) 270°C, (b) 450°C and (c) 630°C.

Figure 3a shows the bulk-EDS spectra of the ZnS nanostructure grown at 270°C. The EDS spectrum indicates that besides Zn and S, the samples contain a significant amount of potassium, gold and oxygen. Fig. 3b shows the typical bulk-EDS spectrum of the sample ZnS sample grown at 630ºC. This sample contains a large amount of arsenic and gallium, besides a significant amount of oxygen that allows forming the ZnO. The results of such measurements for the zinc and sulphur are shown in Table I. From these results is observed that the sample ZnS154 is the one that has a good stoichiometric compound and that starting from it a higher temperature gives a greater presence of zinc in the material and an absence of sulphur. Continuing with the consideration that each unit cell contains two zinc atoms and two sulphur atoms, then when a stoichiometric deviation of ideal unit cell occurs it could establish a correspondence between vacancies or interstices of some of the elements (V_S, V_{Zn}, Zn_i, S_i). From Table I observes that the sample ZnS169 contains a lower sulphur concentration, which indicates that it has a higher structural defects concentration. Fig. 5 shows the ZnS164 thickness measured by SEM, which gives a mean value of 828.3 nm.

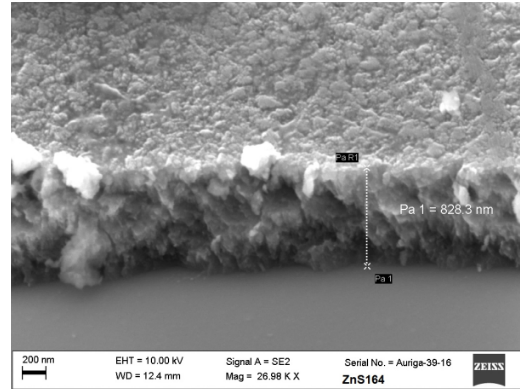

Fig. 5. It shows the thickness of the ZnS164 samples, which was grown at 450ºC.

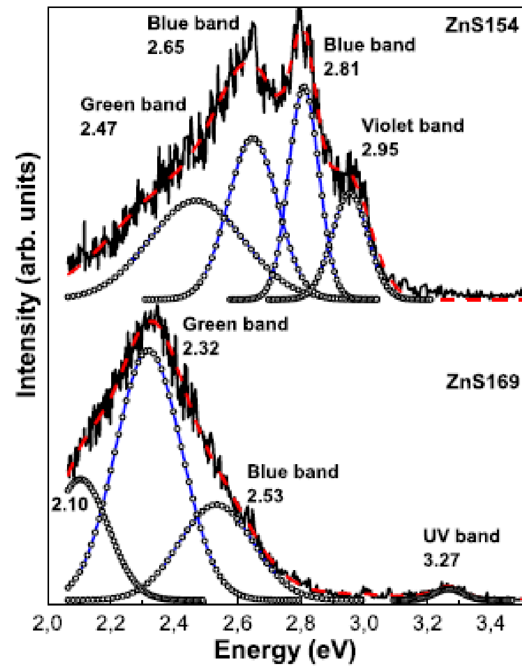

Fig. 6. Room-temperature photoluminiscence spectra of the samples: a) ZnS154 and b) ZnS169.

Figure 6 illustrates room temperature photoluminescence spectra of two intentionally undoped typical ZnS samples ZnS154 and ZnS169, which were grown at lower and higher temperature. The Gaussian fit of the PL spectrum for the ZnS154 sample shows a strong violet peak at 2.95 eV, two strong blue emission peaks ~2.85 and ~2.65 eV, and a green emission peak at 2.47 eV, this sample has a better chemical stoichiometry . Fig. 6b illustrates the Gaussian fit of the PL spectrum in the violet-blue-green-orange region for the ZnS169 sample, which shows a strong green emission at 2.32 with a shoulder at ~2.53 eV in the blue region, a deep level related orange emissions at ~2.10 eV as well as a weak UV band at ~3.27 eV. All the emission bands observed in the present

samples can be explained on the basis of the energy level diagram shown in Fig. 7, an adaptation of the one reported by Goswami and Sen [23]. The analysis is done considering the presence of defect levels due to oxygen ions and interstitial sulphur ions in the system. The transition from oxygen trap levels to valence band in ZnS is reported to be in the UV region around 381 nm whereas the transition from the conduction band to the defect levels of interstitial sulphur ions is reported in the blue region around 440 nm [24]. The interstitial sulphur states marked as I_S in figure can act as deep acceptor levels.

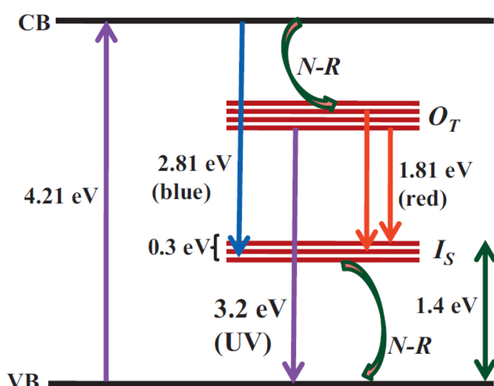

Fig. 7. Energy level diagram explaining the observed emission bands. VB: valence band, CB: conduction band, *N-R*: non-radiative transitions, O_T: oxygen trap levels, and I_S: interstitial sulphur states.

One can comment on the intensity enhancement of the 2.64-3.2 eV range and specifically to the formation of distinct peaks at 2.65, 2.81 and 2.95 eV. In ZnS, the valence band consists largely of s and p orbitals from sulphur while the conduction band is mainly due to s-orbitals of zinc [25]. Although little is known about the energy levels of interstitial sulphur or zinc in ZnS, studies of the green luminescence of CdS powder suggest that interstitial Cd and S vacancies act as 'shallow donors' (electron traps) and interstitial S and Cd vacancies can behave as ' deep acceptor' (hole traps) [26]. If a similar band structure applies to powdered ZnS, the blue emission can be understood as follows. In Figure 7 we illustrate the scheme of the energy states nanocrystalline ZnS band structure and the various processes involved during the PL of these materials. Sulphur vacancies in ZnS generate localized donor sites just below the conduction band. Excitation of these produce a positive charge and conduction band electrons. This localized charge exerts a potential, which can further trap electrons. So upon excitation, S^{2-} vacancies are pumping the electrons into conduction band. Emission occurs when a captured electron recombines with a hole in the valence band or in some acceptor level, which are interstitial sulphur states in this case. These emissions are similar to deep transitions, because here S^{2-} vacancies are behaving like impurity levels. Therefore, blue and violet emissions are attributed lattice defects related to sulphur and zinc vacancy or interstitials.

The green emission is attributed to the radiative recombination of the photogenerated hole with the electron in the singly ionized sulphur vacancy (V_S) level (1.4 eV) [27]. Orange-yellow defect emission, at 2.10 eV, is commonly observed in the ZnO nanostructure, which is responsible for the recombination of a delocalized electron close to the conduction band with a deeply trapped hole in the sulphur interstitial center [28]. The UV emission peak for the ZnS sample grown at 630°C is much less intense compared to the defect luminescence, which indicates the high intrinsic defect density due to low sulphur concentration.

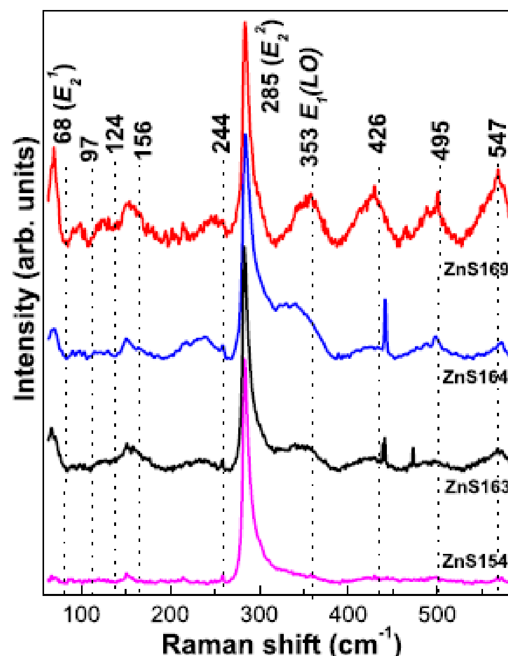

Fig. 8. Raman scattered spectra at 300 K from ZnSlayers for different grown temperatures.

Figure 8 depicts the Raman spectra acquired from the wurtzite-type ZnS films at 300 K. Before comparing the experimental results with previously reported data, one first presents an overview of the first-order Raman scattering from wurtzite ZnS. Wurtzite ZnS unit cell belongs to the C6v point group symmetry with four atoms in a unit cell. The zone-center optical phonons can be classified as the following irreducible representations: $\Gamma_{opt}=A_1+E_1+2E_2+2B_1$. The B_1 modes are silent modes, A_1 and E_1 modes are polar modes and each splits into transverse-optical (TO) and longitudinal-optical (LO) components with different frequencies and both Raman and infrared active, and E_2 modes are nonpolar and Raman active only have two frequencies, the higher-frequency E_2 (high) mode is associated with the sulphur atoms and the lower-frequency E_2 (low) mode is associated with the vibration of the heavy Zn sublattice. The reported frequencies of the Raman active modes of wurtzite ZnS are shown in Table II. The Raman spectra of sample ZnS154 mainly presents as dominant mode E_2, which corresponds at E_2^2 and is sited around 285 cm^{-1} that confirms that the structure is wurtzite type [29]. As is observed the vibrational mode is dominant in this spectrum and is due to that the sample has more sulphur. As the growth temperature is increased the S molar fraction decreases appearing other peaks as E_2^1 at 68 cm^{-1}, which is associated with the vibration of the heavy Zn sublattice, as can see in Fig. 8. The optical phonon mode $A_1(LO) = E_1(LO)$ is reported to have the highest intensity in ZnS wurtzite structure, which was observed at 350 cm^{-1}. The relative intensity of this peak is a

measure of the concentration of crystalline defects in the system. The intensity of the LO phonon mode is found to be comparable with that of the other optical modes in the present case. This is expected in view of the presence of defects in the system, as was inferred from luminescence studies. The LO phonon mode shows a light red shift compared to the reported bulk value. Red shift of the LO phonon mode is known to occur in nanocrystalline systems due to spatial confinement as well as tensile stress due to the presence of defects [30]. Since PL studies indicate the presence of defects in the form of oxygen trap ions and interstitial sulphur ions, the red shift observed here could be a combined effect of confinement as well as strain due to defects in the lattice.

TABLE II. FIRST-ORDER RAMAN FREQUENCIES OF EXPERIMENTAL AND THEORETICAL RESULTS FOR WURTZITE ZNS.

Phonon	Ref. [29]	Ref. [31]	Ref. [32]	Ref. [29]	This work
E_2^1		72	69	76	68
$A_1(TO)$	275	273	272	287	244
$E_1(TO)$	279	273	276	288	285
E_2^2	285	286	286	296	
$E_1(LO)$	353	351	351	347	350
$A_1(LO)$	353	351		350	

Brafman and Mitra have reported that the modes A_1(TO) and E_1(TO) occur at the same wave number 273 cm^{-1} [31]. However, Cheng et al. have calculated theoretically and later confirmed through experimental results that these modes can have different values [29]. The peak observed at 244 cm^{-1} in the present work is attributed to $A_1(TO)$ that is red shift. The composite peak near 166 cm^{-1} can be due to the overlap of peaks at 158 cm^{-1} and 177 cm^{-1}, attributed to two-phonon processes [31].

The selection rules for two-phonon Raman scattering in crystals with the wurtzite structure were reported by Siegle *et al.* [33]. The following general rules can be drawn. (i) Overtones always contain the representation A_1 while combinations belonging to different irreducible representations never contain A_1. (ii) More overtones or combinations become allowed with decreasing symmetry of the point in the BZ considered. (iii) A consequence of the different packing sequence of wurtzite compared to zinc blende is to have the BZ dimension in the cubic (111) direction, which is followed by folding of the phonon branches at the new zone boundary. It uses the phonon dispersion and the symmetry selection rules for two-phonon Raman scattering reported by Siegle *et al.* [40] to identify the second order features in the wurtzite ZnS Raman spectrum, as displayed in Fig. 9, which was obtained of ref. [33]. Accordingly, we can also divide the second order spectra of wurtzite ZnS into three regions: (i) the low frequency region (approximately 0–400 cm^{-1}) dominated by acoustic overtones, (ii) the high-frequency region (540–600 cm^{-1}) formed by optical overtones and combinations, and (iii) the intermediate-frequency region (400–540 cm^{-1}) where optical and acoustic phonon combinations occur.

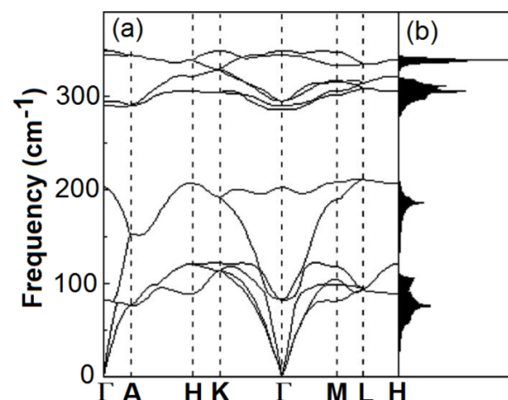

Fig. 9. (a) Phonons band structure and (b) PDOS of wurtzite ZnS [33].

In the low-frequency region [Fig. 8], there are five weak peaks at 78, 107, 134, 166 and 254 cm^{-1}. The peak at 254 cm^{-1} is assigned to LA overtones along M-K, where phonon dispersion is nearly flat (see Fig. 9) and hence the DOS is very high. Above 380 cm^{-1}, we find the acoustic and optical combinations. For instance, the broad weak peak at 436 cm^{-1} can be assigned to TA+LO at L point for flat phonon dispersion. The second-order Raman scattering in the high-frequency region corresponds to LO overtones and combinations involving LO modes. From Fig. 9, we find that the calculated frequencies derived from PDOS and multiplied by 2 shows one main broad band above 540 cm^{-1} which are consistent with the measured Raman spectrum in this region.

IV. CONCLUSIONS

The ZnS films grown by rf magnetron sputtering on GaAs (001) have been studied by XRD, SEM-EDS, room-temperature photoluminescence and. SEM shows that growth temperature can affect the morphology of the films. XRD measurements show the grain size remained almost constant (~32 nm) for the temperature range from 180 to 450°C. XRD analysis reveals that the sample 180°C is polycrystalline and strongly textured, the samples from 270 to 450°C are polycrystalline with hexagonal phases, and the orientation for sample 630°C is believed to be influenced by the substrate orientation. ZnS nanostrucures thus produced exhibit different photoluminescent properties in the visible region as compared to their bulk counterpart.

REFERENCES

[1] Ming Tan, Weiping Cai, Lide Zhang. Optical absorption of ZnS nanocrystals inside pores of silica. J. Appl. Phys. Lett. **71** (1997) 3697–9.

[2] Wei Chen, Zhanguo Wang, Zhaojun Lin, Lanying Lin. Absorption and luminescence of the surface states in ZnS nanoparticles. J. Appl. Phys. **82** (1997) 3111–5.

[3] T. Yokogawa, T. Taguch, Sh. Fujita, M. Satoh. Intense blue-emission band and the fabrication of blue light emitting diodes in I-doped and Ag-ion-implanted cubic ZnS. IEEE Trans Electron Devices **30** (1983) 271–7.

[4] D. Theis, Selected Analytical Tools Yield a Better Insight into Electroluminescent Thin Films). phys. stat. sol. (a), **81** (1984) 647–655

[5] J. Fang, H.P. Holloway, E.J. Yu, S. K. Jones, B. Pathangey, E. Brettschneider, et al. MOCVD growth of non-epitaxial and epitaxial ZnS thin films. J. Appl. Surf. Sci. **70/71** (1993) 701–6.

[6] K. T. Tran, W. Park, W. Tong, M. M. Kyi, K. B. Wagner, J. C. Summers. Photoluminescence properties of ZnS epilayers. J. Appl. Phys. **81** (1997) 2803–9.

[7] G. Shimaoka, T. Arakawa, Y. Suzuki. Electron induced epitaxy of cubic ZnS on GaAs (100) surfaces. J. Appl. Surf. Sci. **212/213** (2003) 694–700.

[8] B. Greengerg, K. W. Zwicker, I. Cadoff. ZnS epitaxy on sapphire {110}. J. Thin Solid Films **141** (1986) 89–97.

[9] J. W. Cook Jr, B. D. Eason, P. R. Vaudo, F. J. Schetzina. Molecular-beam epitaxy of ZnS using an elemental S source. J. Vac. Sci. Technol. B **10** (1992) 901–4.

[10] J. Ihanus, M. Ritala, M. Leskela¨, T. Prohaska, R. Resch, G. Friedbacher, et al. AFM studies on ZnS thin films grown by atomic layer epitaxy. J. Appl. Surf. Sci. **120** (1997) 43–50.

[11] C. W. Wang, T. J. Sheu, Y. K. Su, M. Yokoyama. The study of aging mechanism in ZnS: Mn thin-film electroluminescent devices grown by MOCVD. J. Appl. Surf. Sci. **113/114** (1997) 709–13.

[12] P. Prete, N. Lovergine, M. Masser, C. Zanotti-Fregonora, A. M. Mancini. Diethyldisulphide as sulphur precursor for the low temperature metalorganic vapour-phase epitaxy of ZnS: growth, morphology and cathodoluminescence. J. Crystal Growth **204** (1999) 29–34.

[13] T. K. Hillie, C. Current, H. C. Swart. ZnS thin films grown on Si (100) by XeCl pulsed laser ablation. J. Appl. Surf. Sci. **177** (2001) 73–7.

[14] N. Kumbhojkar, V. V. Nikesh, A. Kshirsagar, S. Mahamuni. Photophysical properties of ZnS nanoclusters. J. Appl. Phys. **88 (**2000) 6260.

[15] B. Salazar-Hernandez, M. A. Vidal, H. Navarro-Contreras, R. Asomoza, A. Merkulov. Excitonic transitions in(GaAs)i.x(Ge_2)x/GaAs multilayers grown by magnetron sputtering. J. Appl. Phys. Lett. **72** (1998) 94–6.

[16] S. F. Chichibu, T. Yoshida, T. Onuma, H. Nakanishi. Helicon-wave-excited-plasma sputtering epitaxy of ZnO on sapphire (0001) substrates. J. Appl. Phys. **91** (2002) 874–7.

[17] A. Boudghene Stambouli, S. Hamzaoui, M. Bouderbala. Blue emitting ACPEL devices based upon ZnS:Tm, Li. Thin Solid Films **283** (1996) 204–8.

[18] K. Hideki, Y. Yoji, M. Yukiniro, T. Yukihisa. ZnS: Mn thin films electroluminescencent devices prepared by metalorganic chemical vapor deposition. J. Crystal Growth **169** (1996) 33–9.

[19] B. E. Warren. X-Ray diffraction. New York: Dover; 1990.

[20] S. Radhu, C. Vijayan. Observation of red emission in wurtzite ZnS nanoparticles and the investigation of phonon modes by Raman spectroscopy. Materials Chemistry and Physics **129** (2011) 1132– 1137

[21] W. Q. Peng, G. W. Cong, S. C. Qu, Z. G. Wang. Synthesis of shuttle-like ZnO nanostructures from precursor ZnS nanoparticles. Nanotechnology **16** (2005) 1469.

[22] X. D. Gao, X. M. Li, W. D. Yu. Structure and UV photoluminescence of nanocrystalline ZnO films prepared by thermal oxidation of ZnS films. Mater. Sci. Eng. B **113** (2004) 274.

[23] N. Goswami, P. Sen, Photoluminescent properties of ZnS nanoparticles prepared by electroexplosion of Zn Wires. J. Nanopart. Res. 9 (2007) 513.

[24] V. N. Do, N. T. Tuan, D. Q. Trung, N. D. Kien, N. D. Chien, P. T. Huy. One-dimensional fabricated by oxidizing ZnS nanowires Mater. Lett. 64 (2010) 1650.

[25] Curie D., 1963. Luminescence in crystals (Methuen, London, chapters 4 and 5).

[26] I. Uchida. Green Edge Emission in CdS. J. Phys. Soc. Jpn. **21** (1966) 645.

[27] K. Vanheusden, W. L. Warren, C. H. Seager, D. R. Tallant, J. A. Voigt. Mechanisms behind green photoluminescence in ZnO phosphor powders. J. Appl. Phys. **79** (1996) 7983

[28] Y. W. Heo, D. P. Nortona, S. J. Pearton, Origin of green luminescence in ZnO thin film grown by molecular-beam epitaxy. J. Appl. Phys. **98** (2005) 073502

[29] Y. C. Cheng, C. Q. Jin, F. Gao, X. L. Wu, W. Zhong, S. H. Li, and Paul K. Chu. Raman scattering study of zinc blende and wurtzite ZnS. J. Appl. Phys. **106** (2009) 123505.

[30] A. Tanaka, O. Seinosuke, T. Arai. Low-frequency Raman scattering from CdS microcrystals embedded in a germanium dioxide glass matrix. Phys. Rev. B: 47 (1993) 1237.

[31] O. Brafman, S.S. Mitra, Raman Effect in Wurtzite- and Zinc-Blende-Type ZnS Single Crystals. Phys. Rev. 171 (1968) 931

[32] J. Schneider and R. D. Kirby. Raman Scattering from ZnS Polytypes. Phys. Rev. B 6, 1290 (1972)

[33] H. Siegle, G. Kaczmarczyk, L. Filippidis, A. P. Litvinchuk, A. Hoffmann, and C. Thomsen. Zone-boundary phonons in hexagonal and cubic GaN. Phys. Rev. B **55**, 7000 (1997).